JACS
JOURNAL OF THE AMERICAN CHEMICAL SOCIETY
Article
pubs.acs.org/JACS

Experimental and Computational Insights into the Stabilization of Low-Valent Main Group Elements Using Crown Ethers and Related Ligands

Charles L. B. Macdonald,*[,†] Rajoshree Bandyopadhyay,[†] Benjamin F. T. Cooper,[†] Warren W. Friedl,[†] Aaron J. Rossini,[†] Robert W. Schurko,[†] S. Holger Eichhorn,[†] and Rolfe H. Herber[‡]

[†]Department of Chemistry and Biochemistry, University of Windsor, Windsor, Ontario N9B 3P4, Canada
[‡]Racah Institute of Physics, The Hebrew University of Jerusalem, Jerusalem 91904, Israel

Supporting Information

ABSTRACT: A series of tin(II) triflate and chloride salts in which the cations are complexed by either cyclic or acyclic polyether ligands and which have well-characterized single-crystal X-ray structures are investigated using a variety of experimental and computational techniques. Mössbauer spectroscopy illustrates that the triflate salts tend to have valence electrons with higher s-character, and solid-state NMR spectroscopy reveals marked differences between superficially similar triflate and chloride salts. Cyclic voltammetry investigations of the triflate salts corroborate the results of the Mössbauer and NMR spectroscopy and reveal substantial steric and electronic effects for the different polyether ligands. MP2 and DFT calculations provide insight into the effects of ligands and substituents on the stability and reactivity of the low-valent metal atom. Overall, the investigations reveal the existence of more substantial binding between tin and chlorine in comparison to the triflate substituent and provide a rationale for the considerably increased reactivity of the chloride salts.

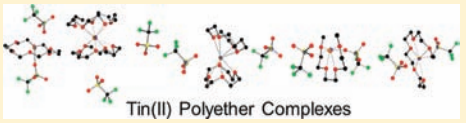

1. INTRODUCTION

The chemistry of main group elements in low oxidation or valence states[1,2] has been an area of active research and discovery over the last few decades[3] that has contributed significantly to the "renaissance" of main group chemistry,[4] and is projected to play a significant role in the future of the field.[5] Low oxidation state compounds are of interest because the unusually electron-rich nature of the species often results in dramatically different chemical behavior and structural features in comparison to analogous compounds that contain the element in a more typical oxidation state. In fact, their unique properties can render low oxidation state species appropriate for uses ranging from new reagent and ligand chemistry,[6] to catalysis (or as models for catalysts),[7] and even to function as materials precursors[8,9] or as models for the formation of nanoscale and bulk materials.[10,11]

As has often been the case for low-coordinate and/or highly reactive species, the judicious design of ligands has proven crucial to the successful isolation of species under typical laboratory conditions. Most of the ligands designed to stabilize otherwise-reactive molecular fragments have featured the use of either steric bulk (e.g., terphenyl ligands[12]) to provide a kinetic barrier to reactivity or donor groups to provide electron density to formally vacant orbitals. Often, as in the case of α-diimino ligands, β-diketiminate ligands, and related nitrogen-based chelating ligands, both steric and electronic stabilization may be provided by the ligand.[13−17]

As an alternative approach to the stabilization of low-valent main group species, we have recently investigated the use of multidentate ligands featuring numerous weak donors and no strong covalent bonds. In particular, we have explored the use of crown ethers as ligands for the stabilization and solubilization of low-valent species from groups 13 and 14, and others have also found that such ligands may be used to isolate interesting mixed-valent[18] and higher valent species.[19] During the course of our investigations, we have made a number of surprising and sometimes puzzling observations. For example, as illustrated in Scheme 1, whereas the free salt [In][OTf] is stable in the presence of halocarbon solvents such as CH_2Cl_2 and $CHCl_3$,[20] the [18]crown-6 ligated variant of the salt [In([18]crown-6)][OTf] rapidly inserts into the C−Cl bonds of such solvents.[21,22] However, the corresponding salt [In([15]crown-5)$_2$][OTf], containing the sandwich-like cation, appears to be inert to such oxidative addition chemistry.[23] In contrast, while [In][OTf] decomposes rapidly in THF, the crown-ether complexes are stable in that solvent. Furthermore, whereas [In([18]crown-6)][OTf] is a stable and readily isolated salt that exists as a contact ion pair in the solid state,[21,24] all attempts to ligate indium(I) halides using crown ethers, either starting from the halides or by generating them in situ, result in the rapid disproportionation of the material. In fact, fragments of the form "In−X([18]crown-6)" have only been insolated as the donor component in adducts of the type X-([18]crown-6)In→InX$_3$.[25]

Similarly, our studies of the chemistry of the isovalent germanium species revealed marked differences between the corresponding triflate and halide analogues, as illustrated in Scheme 2. The use of the [12]crown-4 ligands resulted in the formation of salts containing sandwich-like dications of the

Received: November 28, 2011
Published: January 31, 2012

   dx.doi.org/10.1021/ja211135s | J. Am. Chem. Soc. 2012, 134, 4332−4345

Scheme 1. Some Observed Reactivity Patterns of Monovalent Indium Halides and Triflate Salts and Their Crown Ether Complexes (X = Cl, Br, I; R = H, Cl)

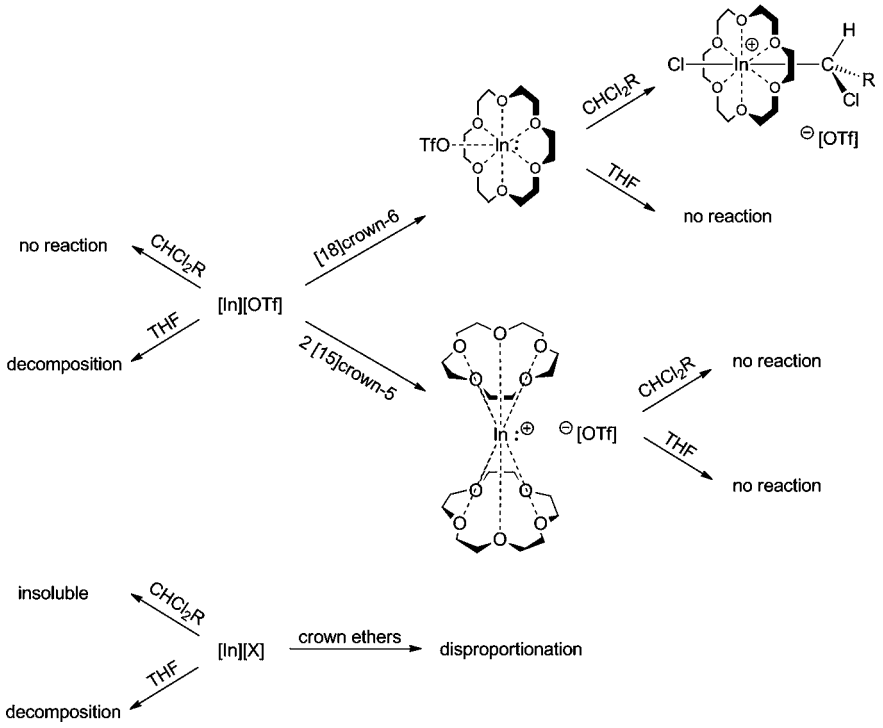

Scheme 2. Illustrations of the Structures of the Complexes Observed from the Treatment of Divalent Germanium Halides or Triflates with Differently Sized Crown Ethers

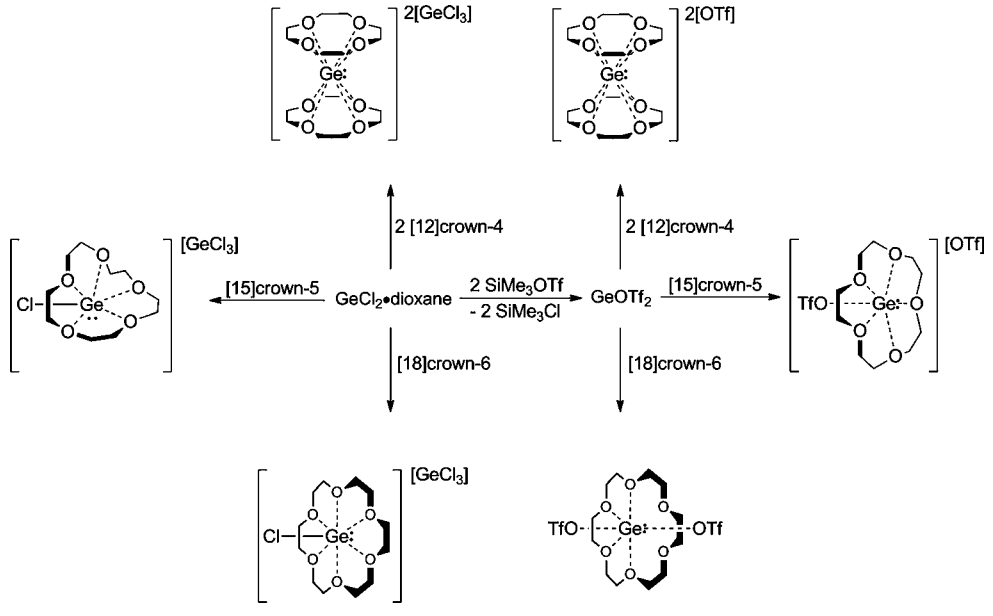

form $[Ge([12]crown-4)_2]^{2+}$ that,[26,27] like the related 222-cryptand encapsulated germanium dication,[28] exhibit no unusual interaction with the counteranions. In stark contrast, the use of the larger crown ethers provided products in which the nature and type of cation−anion interactions have a pronounced effect. For example, whereas the [15]crown-5 adduct of $GeOTf_2$ contains a cation of the form $[Ge([15]crown-5)\cdot OTf]^+$ that features a crown ether with a typical conformation, the cation in the related salt $[GeCl([15]crown-5)][GeCl_3]$ exhibits a crown ether that appears to be "folded".[26]

In this work, we investigate a series of stable tin complexes that are isovalent with the indium(I) and analogous to the germanium(II) complexes described above, and whose spectral and physical properties allow us to obtain valuable insight into their chemistry and electronic structure. We also examine the properties of related complexes of tin(II) with the more flexible glyme-type podand ligands, which are the acyclic analogues of crown ethers, to determine if they are suitable for the stabilization and/or solubilization of low-valent species. More generally, the conclusions we can draw from these studies provide for a

dx.doi.org/10.1021/ja211135s | J. Am. Chem. Soc. 2012, 134, 4332−4345

deeper understanding of the factors that contribute to the stabilization (or activation) of low-valent species, thereby allowing for improvements in the design of ligands suitable for the desired reactivity.

2. EXPERIMENTAL SECTION

2.1. General Methods. All work was carried out using standard inert-atmosphere techniques. All reagents and solvents were obtained from Aldrich or Strem and were used without further purification. Complexes [Sn([18]crown-6)OTf][OTf] (**1**), [Sn([15]crown-5)$_2$][OTf]$_2$ (**2**), and [Sn([12]crown-4)$_2$][OTf]$_2$ (**3**) were prepared as described previously.[29] The salt [SnCl([18]crown-6][SnCl$_3$] (**6**) was prepared by a modification of the reported procedure.[30,31] Solvents were dried on a series of Grubbs'-type columns and were degassed prior to use.[32] C_6D_6 and CD_2Cl_2 were distilled over CaH_2 and then stored over 4 Å molecular sieves. Unless otherwise noted, solution NMR spectra were recorded at room temperature on either Bruker DPX 300 MHz or DRX 500 MHz spectrometers. Chemical shifts are reported in ppm, relative to external standards ($SiMe_4$ for ^{1}H and ^{13}C; $CFCl_3$ for ^{19}F; $SnMe_4$ for ^{119}Sn). Elemental analyses were performed at the Centre for Catalysis and Materials Research at the University of Windsor.

2.2. Synthetic Procedures. Each of the glyme complexes was prepared using the following procedure. A solution of the desired glyme in acetonitrile (ca. 1 mL) was added dropwise to a solution of Sn(OTf)$_2$ in the same solvent (50 mL). The resultant colorless solution was stirred overnight, and subsequently all volatile components were removed under reduced pressure to afford a colorless liquid. The liquid was rinsed and sonicated with a 1:5 mixture of ether:pentane to yield a cream colored solid characterized in each case as the target 1:1 glyme complex. Crystalline material suitable for examination by single-crystal X-ray diffraction was obtained by the slow evaporation of a saturated solution of this material from a 50:50 mixture of THF and toluene.

*Data for Sn(OTf)$_2$·triglyme (**4**).* Reagents: triglyme (0.304 mL, 1.68 mmol); Sn(OTf)$_2$ (350 mg, 0.840 mmol). Product: Sn(OTf)$_2$·triglyme (**4**) (405 mg, 0.524 mmol, 62%). Anal. Calcd for $C_{10}H_{18}F_6O_{10}S_2Sn$ (fw 595.05 g mol^{-1}): C, 20.14; H, 3.04. Found: C, 20.08; H, 3.11. ^{1}H NMR (CD_3CN, δ, ppm): 3.56 (s, 6H), 3.76 (m, 4H), 4.02 (m, 8H). ^{13}C NMR{^{1}H} ($CDCl_3$, δ, ppm): 58.4 (s), 69.5 (s), 69.8 (s), 71.5 (s), 119.8 (q). ^{19}F{^{1}H} NMR (CD_3CN, δ, ppm): −79 ppm (s).

*Data for Sn(OTf)$_2$·tetraglyme (**5**).* Reagents: tetraglyme (0.211 mL, 0.960 mmol); Sn(OTf)$_2$ (400 mg, 0.960 mmol). Product: Sn(OTf)$_2$·tetraglyme (**5**) (554 mg, 0.868 mmol, 90%). Anal. Calcd for $C_{12}H_{22}F_6O_{11}S_2Sn$ (fw 639.10 g mol^{-1}): C, 22.50; H, 3.46. Found: C, 22.06; H, 3.60. ^{1}H NMR (CD_3CN, δ, ppm): 3.47 (s, 6H), 3.72 (m, 4H), 3.94 (m, 8H), 4.02 (m, 4H). ^{13}C{^{1}H} NMR ($CDCl_3$, δ, ppm): 58.0 (s), 69.0 (s), 70.0 (s), 70.2 (s), 70.8 (s), 120.0 (q). ^{19}F{^{1}H} NMR (CD_3CN, δ, ppm): −79 ppm (s).

2.3. X-ray Crystallography. The subject crystals were covered in Nujol or Paratone-N, mounted on a goniometer head, and rapidly placed in the dry N_2 cold-stream of the low-temperature apparatus (Kryoflex) attached to the diffractometer. The data were collected using the SMART[33] software on a Bruker APEX CCD diffractometer using a graphite monochromator with Mo Kα radiation (λ = 0.71073 Å). A hemisphere of data was collected for each crystal using a counting times ranging from 10 to 30 s per frame at −100 °C. Details of crystal data, data collection, and structure refinement are listed in Table 1. Data reduction was performed using the SAINT-Plus software,[34] and the data were corrected for absorption using SADABS.[35] The structures were solved by direct methods using SIR97[36] and refined by full-matrix least-squares on F^2 with anisotropic displacement parameters for the nondisordered heavy atoms using SHELXL-97[37] and the WinGX[38] software package, and thermal ellipsoid plots were produced using SHELXTL.[39] The space group assignments and structural solutions were evaluated using PLATON.[40] One of the triflate groups in **4** was disordered, and this disorder was refined using a two-site model in which the corresponding thermal parameters and bond distances in each of the two components were restrained to be similar; the refinement revealed that the occupancy of the most common site is approximately 70%. Powder X-ray diffraction (pXRD) experiments that confirm that the bulk materials are consistent with the single-crystal structures were performed with a Bruker D8 Discover diffractometer equipped with a Hi-Star area detector using Cu Kα radiation (λ = 1.54186 Å).

Table 1. Summary of Crystallographic Data for the Compounds in This Work

compound	Sn(OTf)$_2$·triglyme	Sn(OTf)$_2$·tetraglyme
compound no.	**4**	**5**
empirical formula	$C_{10}H_{18}F_6O_{10}S_2Sn$	$C_{12}H_{22}F_6O_{11}S_2Sn$
formula weight	595.05	639.11
temperature (K)	173(2)	173(2)
wavelength (Å)	0.71073	0.71073
crystal system	monoclinic	monoclinic
space group	$P2_1/n$	$P2_1/c$
a (Å)	8.7518(8)	14.1583(19)
b (Å)	16.1270(14)	10.1383(14)
c (Å)	14.8106(13)	17.040(2)
α (deg)	90	90
β (deg)	101.0220(10)	109.332(2)
γ (deg)	90	90
volume (Å^3)	2051.8(3)	2308.0(5)
Z	4	4
density (g cm^{-3})	1.926	1.839
abs. coeff. (mm^{-1})	1.547	1.385
F(000)	1176	1272
color	colorless	colorless
crystal size (mm^3)	0.3 × 0.2 × 0.2	0.4 × 0.4 × 0.3
θ range for data collection (deg)	1.89−27.49	1.752−27.50
data/restraints/parameters	4653/49/335	5166/0/291
GOF, S (all data)[a]	1.133	1.198
final R indices [$I > 2\sigma(I)$][b]	0.0395	0.0700
wR2 indices (all data)[b]	0.1114	0.1325
largest diff. peak and hole (e Å^{-3})	1.019 and −0.587	1.586 and −1.005

[a] $S = [\sum w(|F_o|^2 - |F_c|^2)^2]/(n-p)^{1/2}$, where n is the number of reflections and p is the number of parameters used. [b] $R1(F) = \sum(|F_o| - |F_c|)/\sum|F_o|\}$ for reflections with $F_o > 4(\sum(F_o))$. $wR2(F^2) = \{\sum w(|F_o|^2 - |F_c|^2)^2/\sum w(|F_o|^2)^2\}^{1/2}$, where w is the weight given for each reflection.

2.4. Mössbauer Spectroscopy. Temperature-dependent ^{119}Sn Mössbauer effect (ME) spectra were acquired in transmission geometry using a 2mCi ^{119m}Sn source ($CaSnO_3$) as described previously.[41] All isomer shifts (IS) are with respect to the centroid of a room temperature $BaSnO_3$ absorption spectrum, and spectrometer calibration was effected as usual.[42] Temperature monitoring over the extended data acquisition intervals was effected using the Daswin program of Glaberson.[43] To monitor the temperature dependence of the recoil-free fraction (−d ln A/dT), the transmission rate was recorded both before and after each temperature point data acquisition. It should be noted that all of the ME spectra show the presence of an Sn(IV) impurity with a signal at around 0 mm s^{-1}, which is almost certainly a tin(IV) oxide that appears to arise as a result of sample preparation in air.[44]

2.5. Solid-State NMR Spectroscopy. ^{119}Sn and ^{13}C solid-state NMR (SSNMR) spectra were acquired on a Varian Infinity Plus spectrometer with an Oxford 9.4 T wide-bore magnet [$\nu_0(^1H)$ = 399.73 MHz]. Tin chemical shifts were referenced to neat liquid Me_4Sn (δ_{iso} = 0.0 ppm).[45] Carbon chemical shifts were referenced to tetramethylsilane (δ_{iso} = 0.0 ppm) by using the high-frequency peak of adamantane as a secondary reference (δ_{iso} = 38.56 ppm).[46]

All SSNMR experiments were performed on triple resonance 4 mm HXY or double-resonance 4 mm HX Varian/Chemagnetics probe. Magic-angle spinning (MAS) ^{119}Sn SSNMR spectra were acquired

with either direct excitation of ^{119}Sn (π/2-acquire) or variable-amplitude cross-polarization (VACP) from ^{1}H.[47,48] Static (i.e., stationary sample) ^{119}Sn SSNMR spectra were acquired with a variety of pulse sequences, which are indicated in the figures: (i) direct excitation spin echo ($\pi/2-\tau-\pi-\tau-$acquire), (ii) quadrupolar Carr–Purcell Meiboom–Gill (QCPMG),[49] (iii) CP spin echo, and (iv) cross-polarization/Carr–Purcell–Meiboom–Gill (CP/CPMG).[50,51] Echo reconstructed CPMG spectra were obtained by summing the whole echoes of the FIDs in the time domain, followed by Fourier transform and magnitude calculation.[52,53] CP experiments were optimized directly on the individual samples. All spectra were acquired with ^{1}H decoupling using the TPPM decoupling scheme.[54] All ^{1}H–^{119}Sn CP experiments employed 2.15 μs π/2 proton pulses, Hartman–Hahn matching fields of approximately 40 kHz, contact times between 5 and 10 ms, and recycle delays between 2 and 8 s. ^{119}Sn{^{1}H} direct excitation experiments employed recycle delays of 10–20 s and π/2 pulses of 1.55 μs, and between 80 and 2000 transients were collected. Static and MAS ^{119}Sn SSNMR spectra were simulated with the WSolids program,[55] which includes Herzfeld–Berger analysis[56] of MAS spectra. The anisotropic CS tensor parameters (Ω and κ) and δ_{iso} were initially obtained from simulations of the MAS ^{119}Sn SSNMR spectra (Figure S1) and refined via simulations of static ^{119}Sn SSNMR spectra. For **6**, the CS tensor parameters were obtained exclusively from simulations of the MAS ^{119}Sn SSNMR spectrum. The MAS ^{13}C SSNMR spectra are presented exclusively in the Supporting Information.

2.6. Cyclic Voltammetry. Cyclic voltammetry experiments were conducted using a Bioanalytical Systems Electrochemical Analyzer BAS100B/W instrument employing a one-compartment, three-electrode cell with a 3 mm diameter glassy carbon working electrode, a platinum counter electrode, and an $Ag/AgNO_3$ (0.1 M in MeCN) reference electrode. The voltammograms were recorded for solutions of each of the complexes in dichloromethane using electrochemical grade $[NBu_4][PF_6]$ (0.1 M) as the supporting electrolyte. A variety of scan rates were examined, and the results reported herein were recorded at 100 mV s^{-1}.

2.7. Computational Investigations. *DFT and MP2 Calculations of Electronic Structure and Population Analyses.* All of the computational investigations were performed using the Shared Hierarchical Academic Research Computing Network (SHARCNET) facilities (www.sharcnet.ca), with either the Gaussian 03[57] or Gaussian 09[58] program suite. Geometry optimizations have been calculated using density functional theory (DFT), specifically implementing the B3PW91 method[59,60] in conjunction with Stuttgart/Dresden (SDD) quasi-relativistic effective core pseudopotential and basis set for Sn[61] and the 6-31G(d) basis set for all other atoms. The geometry optimizations were not subjected to any symmetry restrictions, and each stationary point was confirmed to be a minimum having zero imaginary vibrational frequencies. Single-point calculations were conducted at the MP2 level using the same basis set on models in which the heavy atom positions were those observed in the solid-state structures, and hydrogen atoms were placed in appropriate geometrically calculated positions (with C–H bond lengths set to 1.07 Å) using Gaussview 3.0. Population analyses were conducted using the Natural Bond Orbital (NBO)[62] implementation included with the Gaussian packages. The magnitudes of the lowest-energy electronic transitions were computed using time-dependent DFT (TD-DFT) at the B3PW91/dgdzvp[63,64] level of theory using the single-point geometries. Plots of molecular orbitals and electron densities were generated using MOLDEN.[65]

DFT Calculations of ^{119}Sn NMR Parameters. Theoretical calculations were performed with the EPR and NMR module[66–68] of the Amsterdam Density Functional (ADF) program suite.[69–71] The VWN-BP functional was used for electron exchange and correlation for all calculations.[72–74] Relativistic effects (including spin–orbit) were taken into account with the zeroth-order regular approximation (ZORA).[75–79] All-electron gauge including atomic orbitals (GIAO)[80] triple-ζ doubly polarized (TZ2P) basis sets were employed on all atoms. Additional calculations employing an all-electron quadruple-ζ quadruple polarized (QZ4P) basis set on Sn and the TZ2P basis set on all other atoms were also attempted. The calculations were performed using the single-point models described above or, where indicated, using the B3PW91 geometry optimized structures. The NMR calculations on the models of the [12]crown-4 and [15]crown-5 tin(II) triflate complexes **2** and **3** included only the coordinated crown ether ligands and carried an overall +2 charge (i.e., the triflate anions were not included). NMR calculations on the model for the [18]crown-6 tin(II) triflate complex **1** were performed on a neutral unit including the crown ether ligand and the two nearest triflate ligands. The isotropic magnetic shielding (σ_{iso}) values of $SnMe_4$ (with the B3PW91 optimized geometry) calculated at the corresponding level of theory were used to convert the calculated principal magnetic shielding values (σ_{ii}) to chemical shift (δ_{ii}) values (see Table 3).

3. RESULTS AND DISCUSSION

3.1. Syntheses and Structural Details. As we noted previously, well-defined, crystalline complexes of $Sn(OTf)_2$ with crown ethers are readily prepared through the treatment of tin(II) triflate with the appropriate stoichiometry of the cyclic polyether [18]crown-6, [15]crown-5, or [12]crown-4 (Figure 1). Although

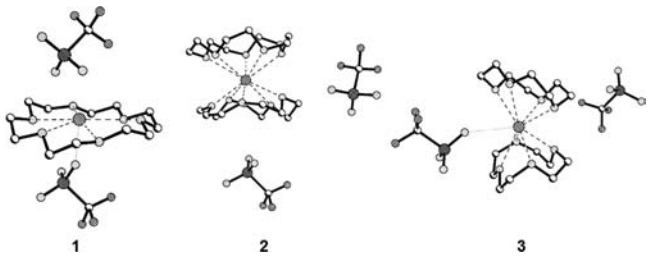

Figure 1. Solid-state structures of [Sn([18]crown-6)OTf][OTf], **1**, $[Sn([15]crown-5)_2][OTf]_2$, **2**, and $[Sn([12]crown-4)_2][OTf]_2$, **3**, illustrating the different structural types adopted by the differently sized cyclic polyether ligands. Dashed lines are used to emphasize coordination environment of the tin atom attributable to the oxygen atoms of the crown ether ligand, and the dotted lines indicate the closest tin–anion contacts.

a detailed description of the structures has been reported,[29] a summary of the important features of these structures is presented so that the reader may appreciate the structure–property relationships that are inferred from the physical, spectroscopic, and computational investigations presented in the following sections.

The 1:1 adduct of $Sn(OTf)_2$ with [18]crown-6, **1**, exhibits a structure in which the tin atom is "belted" by the crown ether in a manner reminiscent of s-block metal crown ether complexes. Overall, the complex appears to exist as a salt of the form [Sn([18]crown-6)OTf][OTf], in which there is one tin-bound triflate substituent (Sn–O: 2.282(6) Å) and one "free" triflate anion (Sn–O: 2.596(9) Å); such an arrangement is at least superficially similar to the structure of [Sn([18]-crown-6)Cl][$SnCl_3$].[31]

The smaller crown ethers, [15]crown-5 and [12]crown-4, are too small to accommodate the tin atom within the crown ether cavity, and thus both form 2:1 sandwich-like complexes with the divalent metal. In the case of **2**, there appears to be no interactions between the triflate anions and tin atom in the roughly centrosymmetric $[Sn([15]crown-5)_2]^{2+}$ dication. In contrast, in salt **3**, the smaller [12]crown-4 ligands are not large enough to completely encapsulate the tin atom, and the cation is best described as being a bent "crown"-sandwich complex. The open wedge of the cation appears to allow for the interaction of the tin atom with an adjacent triflate anion; however, the very long

dx.doi.org/10.1021/ja211135s | J. Am. Chem. Soc. 2012, 134, 4332–4345

Sn−O distance of 3.119(4) Å and the metrical parameters of both the cation and the triflate group suggest that this is a very weak interaction that does not noticeably perturb the structures of the component ions.[29]

Given that the size of the crown ether ring clearly plays a role in the composition and structure adopted by low-valent complexes from groups 13 and 14, we rationalized that glyme-type podand ligands might be superior for the stabilization and/or solubilization of low-valent species: the absence of the constraints associated with being cyclic renders glymes more flexible so that they may adjust their binding to the most favorable arrangement. In this vein, we observed that the treatment of $Sn(OTf)_2$ with triglyme or tetraglyme in acetonitrile results in the formation of the 1:1 complexes $Sn(OTf)_2$·triglyme, **4**, or $Sn(OTf)_2$·tetraglyme, **5**, in quantitative yield on the basis of NMR spectroscopy and isolated in reasonable crystalline yield and high purity (as assessed by microanalysis and pXRD). It is noteworthy that, in contrast to all of the crown ether complexes described above, the ^1H and ^{13}C NMR signals for the glyme ligand are markedly different upon complexation and confirm the formation of complex in solution. However, like all of the crown ether complexes, no identifiable ^{119}Sn solution NMR signals for the complexes could be detected.

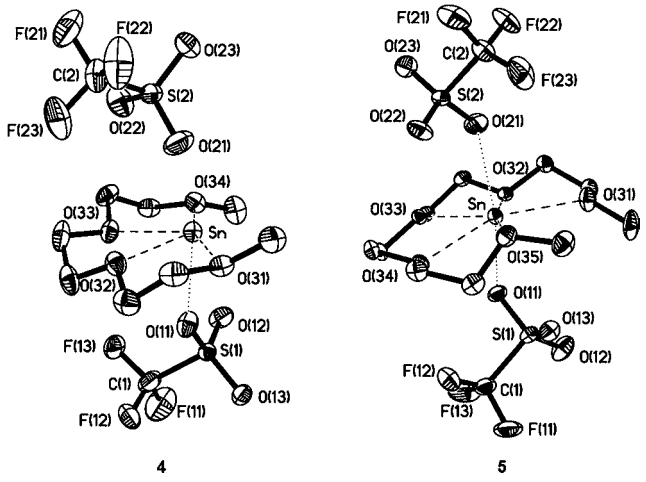

Figure 2. Solid-state structures of $Sn(OTf)_2$·triglyme, **4**, and $Sn(OTf)_2$·tetraglyme, **5**; thermal ellipsoids are drawn to depict the 30% probability surface, and all hydrogen atoms are omitted for clarity. For compound **4**, only the highest-occupancy component of the disordered triflate group (containing S(1), O(11), etc.) is depicted. Selected metrical parameters including distances (Å) and angles (deg): **4**, Sn−O(11), 2.331(6); Sn−O(21), 2.741(6); Sn−O(31), 2.511(3); Sn−O(32), 2.378(3); Sn−O(33), 2.454(3); Sn−O(34), 2.725(3); S(1)−O(11), 1.471(5); S(1)−O(12), 1.401(5); S(1)−O(13), 1.430(15); S(2)−O(21), 1.425(4); S(2)−O(22), 1.420(4); S(2)−O(23), 1.436(3); O(11)−Sn−O(21), 166.4(4); **5**: Sn−O(11), 2.408(5); Sn−O(21), 2.519(6); Sn−O(31), 2.664(6); Sn−O(32), 2.436(4); Sn−O(33), 2.396(4); Sn−O(34), 2.568(5); Sn−O(35), 2.968(5); S(1)−O(11), 1.466(5); S(1)−O(12), 1.421(5); S(1)−O(13), 1.430(5); S(2)−O(21), 1.443(6); S(2)−O(22), 1.416(5); S(2)−O(23), 1.415(5); O(11)−Sn−O(21), 145.2(2).

Crystals suitable for examination by X-ray diffraction were obtained by the slow evaporation of solutions of **4** or **5** in 1:1 mixtures of THF and toluene; **4** crystallizes in the space group $P2_1/n$ with one formula equivalent comprising the asymmetric unit (Figure 2). Examination of the pertinent metrical parameters suggests that complex **4** appears to be similar to the [18]crown-6 complex **1** in several ways. The compound is a 1:1 complex in which the ligand binds the tin atom in a belt-like manner and there appear to be two distinct triflate environments: one with a longer Sn−O distance of 2.741(6) Å and metrical parameters consistent with a "free" triflate anion and the other with a considerably shorter Sn−O distance of 2.331(6) Å and very slightly perturbed S−O distances. The $Sn-O_{glyme}$ distances range from 2.378(3) to 2.725(3) Å of which three are roughly 2.5 Å or less and one is substantially longer; this is somewhat in contrast to **1** in which there are two short, two intermediate, and two long distances.

The tetraglyme complex **5** crystallizes in the space group $P2_1/c$ with one formula equivalent comprising the asymmetric unit (Figure 2). As in **4**, the glyme ligand in **5** binds the metal in a belt-like arrangement, and the $Sn-O_{glyme}$ distances range from 2.397(5) to 2.968(5) Å. The distribution of these ligand to metal contacts is more reminiscent of **1** in that there are two at shorter distances, two somewhat further away, and one with a considerably longer Sn−O distance. In contrast to **1** and **4**, there is a much smaller range of distances between the tin atom and the triflate anions in complex **5**: one triflate has a closest Sn−O distance of 2.408(5) Å, and the other has a closest contact at 2.519(6) Å. The S−O distances within each of the triflate fragments in **5** are consistent with those of a very slightly perturbed anion and suggest that the contact ion pair description is applicable to each triflate group.

Overall, the large variation in the coordination spheres around the tin atoms in complexes **1**−**5**, including apparently very different levels of interactions between the tin atoms and both the anions and the ligands, suggests that these systems should be excellent models to provide insight into the nature of the ligand-dependent reactivity differences outlined in the Introduction. Furthermore, we prepared the known salt $[Sn([18]crown-6)Cl][SnCl_3]$,[30,31] **6**, which has a structure that is superficially similar to **1** (the solid-state structure adopted by our samples of **6** was confirmed by pXRD to be consistent with that reported in the Cambridge Structural Database[81]), in an effort to rationalize the very different chemistry that is often observed for comparable low-valent halide and triflate analogues.

3.2. Mössbauer Spectroscopy. Samples of each of the complexes **1**−**6** were analyzed by ^{119}Sn Mössbauer spectroscopy. Representative spectra are illustrated in Figure 3, and the isomer shifts (IS) and quadrupolar splittings (QS) at 90 K extracted from each of the spectra are collected in Table 2.

As one would anticipate, in each of the spectra for the various complexes of $Sn(OTf)_2$, the major resonance is indicative of the presence of tin(II); however, there are several important observations that are apparent upon more detailed analysis. For example, it is clear that the magnitude of the isomer shift (IS) is directly correlated with the degree of spherical symmetry of the coordination sphere about each tin atom. The largest value of IS (4.504(6) mm s^{-1}) is found for complex **2** in which the cation has almost D_5 point symmetry with an arrangement of oxygen atoms that is distributed approximately centrosymmetrically around the tin cation. Such a structure suggests that the two valence electrons on the Sn(II) atom occupy the 5s orbital almost exclusively, which is consistent with the large magnitude of the IS. The distorted crown-sandwich structure of the cation in **3** exhibits the next largest isomer shift, whereas the IS magnitudes are the smallest for species **1**, **4**, and **5**, which feature less symmetrical Sn bonding environments. The IS values for each of the triflate complexes are consistent with the Sn−ligand interaction being primarily ionic (rather than covalent)

dx.doi.org/10.1021/ja211135s | J. Am. Chem. Soc. 2012, 134, 4332−4345

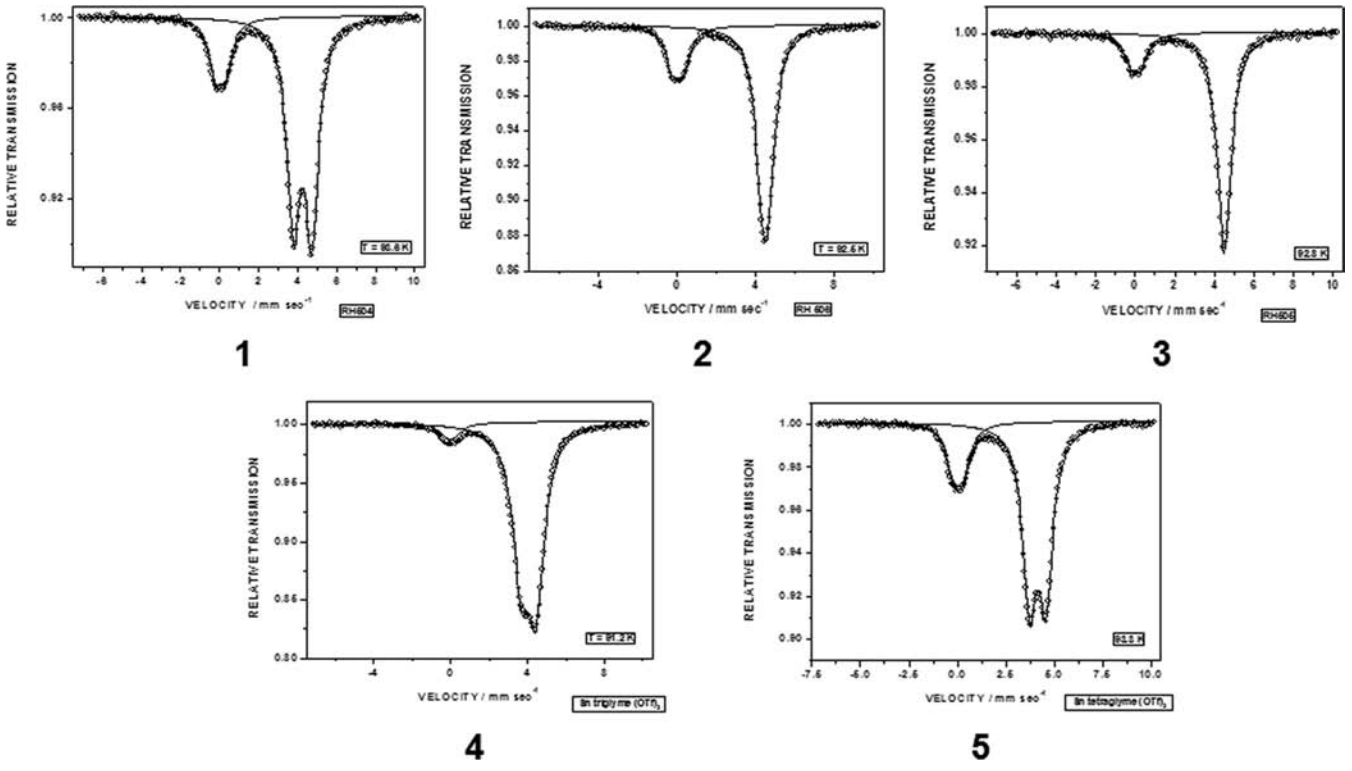

Figure 3. ^{119}Sn Mössbauer spectra for the triflate complexes **1**−**5** reported in this work. The peak at 0 mm s^{-1} is a Sn(IV) impurity.[44]

Table 2. Summary of ^{119}Sn Mössbauer Spectroscopic Results for the Compounds Reported in This Work

complex	IS(90)[a] mm s^{-1}	QS(90)[a] mm s^{-1}	−d ln A/dT[b] K^{-1} × 10^{-3}	reference	QS(calcd)[c] mm s^{-1}
[Sn([18]crown-6)OTf][OTf] (**1**)	4.267(6)	0.924(6)	22.94	this work	−0.622
[Sn([15]crown-5)$_2$][OTf]$_2$ (**2**)	4.504(6)	0.0(1)	19.36	this work; cf., refs 82,83	0.201
[Sn([12]crown-4)$_2$][OTf]$_2$ (**3**)	4.480(6)	0.340(6)	16.85	this work	0.359
Sn(OTf)$_2$·triglyme (**4**)	4.056(6)	0.794(6)	22.09	this work	0.433
Sn(OTf)$_2$·tetraglyme (**5**)	4.062(6)	0.789(6)	18.07	this work	−0.757
Sn(OTf)$_2$	4.15	0.84		84	
[SnCl([18]crown-6)]$^+$ (**6** cation)	3.83(2)	2.78(2)		this work and refs 30,31	−2.588
[SnCl$_3$]$^-$ (**6** anion)	3.45(2)	0.89(2)		this work and refs 30,31	−1.626

[a]Isomer shift (IS) and quadrupole splitting (QS) at 90 K for measurements obtained in this work. [b]All of the spectra indicate anisotropic Sn motion, but this effect is not very large. The rapid decrease in the recoil-free fraction with increasing temperature (−d ln A/dT) precludes a more detailed analysis. [c]QS calculated using the ADF method described in the Experimental Section for the complexes examined in this work.

in nature. This assertion is supported by the effective mass calculation on each of the triflate complexes **1**−**5**, which indicate a "vibrating mass" of close to 110 Da, that is, that of a "bare" Sn atom, in every instance. It is also worth noting that the ionic interpretation of the metal−ligand bonding in these complexes is in concordance with the results of XANES investigations of related Ge(II) complexes.[85] In sharp contrast, the 3.83(2) mm s^{-1} value of IS for the crowned cation in the chorine-containing complex **6**, although still characteristic of a Sn(II) atom, is considerably smaller than that (4.267(6) mm s^{-1}) of the structurally similar triflate complex **1**.

The quadrupolar splitting (QS) magnitudes for each of the complexes provide insight into the symmetry of the electric field gradient (EFG) around the tin atoms in each of the complexes and the level of degeneracy of the 5p-type orbitals on Sn that comprise the LUMOs. As one might anticipate on the basis of the structure exhibited by the cation, it is found that the ^{119}Sn Mössbauer spectrum of **2**, which has the most spherically symmetrical distribution of oxygen atoms about the tin atom, consists of a single peak and is thus indicative of a negligible quadrupolar splitting. Although the complex does not conform to perfect cubic symmetry (which would require QS = 0), the arrangement of the 10 oxygen atoms in two staggered pentagons provides a geometry that roughly emulates a centrosymmetric dodecahedron in which one-half of the vertices are occupied.[86] Provided that the charges at each vertex are identical, the EFG for such a polyhedron is predicted to be 0 at the center of symmetry.[87−89] Somewhat despite its appearance in Figure 3, analysis of the spectrum of **3** reveals that it is a doublet with a QS magnitude of 0.340(6) mm s^{-1}. The relatively small size of the quadrupolar splitting is consistent with the bent-sandwich structure of the complex in which there is also a nearly spherically symmetrical arrangement of the oxygen atoms about the tin atom. The spectra of triflate complexes **1**, **4**, and **5** each feature obvious doublet signals with QS values consistent with less spherically symmetrical Sn coordination environments and significant Sn EFGs. The largest value of QS for any of the triflate complexes (0.924(6) mm s^{-1}) is observed for compound **1**, which features an asymmetrical arrangement of coordinating atoms around Sn, and, most importantly,

dx.doi.org/10.1021/ja211135s | J. Am. Chem. Soc. 2012, 134, 4332−4345

possesses the shortest Sn−OTf contact found in **1**−**5**. Again, it should be emphasized that the QS magnitude observed for the cation of the chlorinated species **6** (2.78(2) mm s^{-1}) is approximately 3 times as large as that of **1** and highlights the dramatically different properties of the two analogous salts despite the apparent similarity of their structures. Finally, it should be noted that the trends in the experimental magnitudes of the QS values are predicted with reasonable accuracy by DFT calculations using models derived from the solid-state structures, as indicated in Table 2.

3.3. Solid-State NMR Spectroscopy. ^{119}Sn SSNMR spectroscopy can act as a powerful probe of the molecular and electronic structure of Sn complexes.[90,91] ^{119}Sn chemical shift tensors are sensitive to the both the symmetry and the energies of occupied and virtual molecular orbitals with Sn character and are useful for confirming that single-crystal X-ray structures are representative of the bulk material. Each of the tin triflate complexes **1**−**5**, the chlorinated analogue **6**, and the synthetic precursors, tin dichloride and tin ditriflate, were examined using solid-state ^{119}Sn NMR (Figures 4−6, S1, and S2). The ^{119}Sn SSNMR spectra of **1**−**6** confirm that all samples are of high purity and do not indicate the presence of any tin-containing impurities.

The isotropic tin chemical shifts (δ_{iso}) (Table 3) for all of the triflate complexes indicate that the ^{119}Sn nuclei are highly shielded, which may arise from (1) the ionic nature of the complexes, which feature no strongly covalent bonds to the tin atoms, and (2) the symmetry of the HOMO on the Sn atom (the "lone pair", which is best approximated as being a filled 5s orbital) and the low-lying virtual orbitals on Sn (approximated by the vacant 5p-type orbitals). Either or both of these factors result in a situation in which the paramagnetic σ_p component in Ramsey's treatment of shielding[93−95] ($\sigma_{tot} = \sigma_d + \sigma_p$) is likely to be small (this component normally is responsible for deshielding). In contrast, the δ_{iso} observed for both the cations and the anions in the chlorinated analog **6** indicate that the ^{119}Sn nuclei are considerably deshielded, which is reflective of the existence of covalent Sn−Cl bonds. Moreover, the observation of fine structure in the MAS ^{119}Sn SSNMR spectrum of **6** is attributed to indirect spin−spin coupling and residual dipolar coupling to quadrupolar $^{35/37}$Cl nuclei,[96] which is also consistent with the presence of covalent Sn−Cl bonds (Figure 5).

The spans (Ω) of the ^{119}Sn SSNMR spectra are another feature that clearly differentiate the triflate complexes (**1**−**5**) from the chlorinated analogue (**6**), and appear to be related to the Mössbauer QS values. Within the triflate complexes, the salt with the most spherically symmetrical Sn environment, **2**, exhibits the smallest Ω (and QS). Complexes **1**, **3**, **4**, and **5** all have a larger Ω (and correspondingly larger QS values). The much larger Ω measured for the cation in **6** dwarfs those for all of the triflate complexes, again demonstrating that there are fundamental differences between the seemingly analogous chloride and triflate complexes. In this regard, it is well-known from ^{119}Sn SSNMR studies of Sn(II) complexes[97−99] and ^{207}Pb SSNMR studies of Pb(II) complexes,[100−102] that as the p-orbital character of the HOMO metal centered "lone pair" increases,

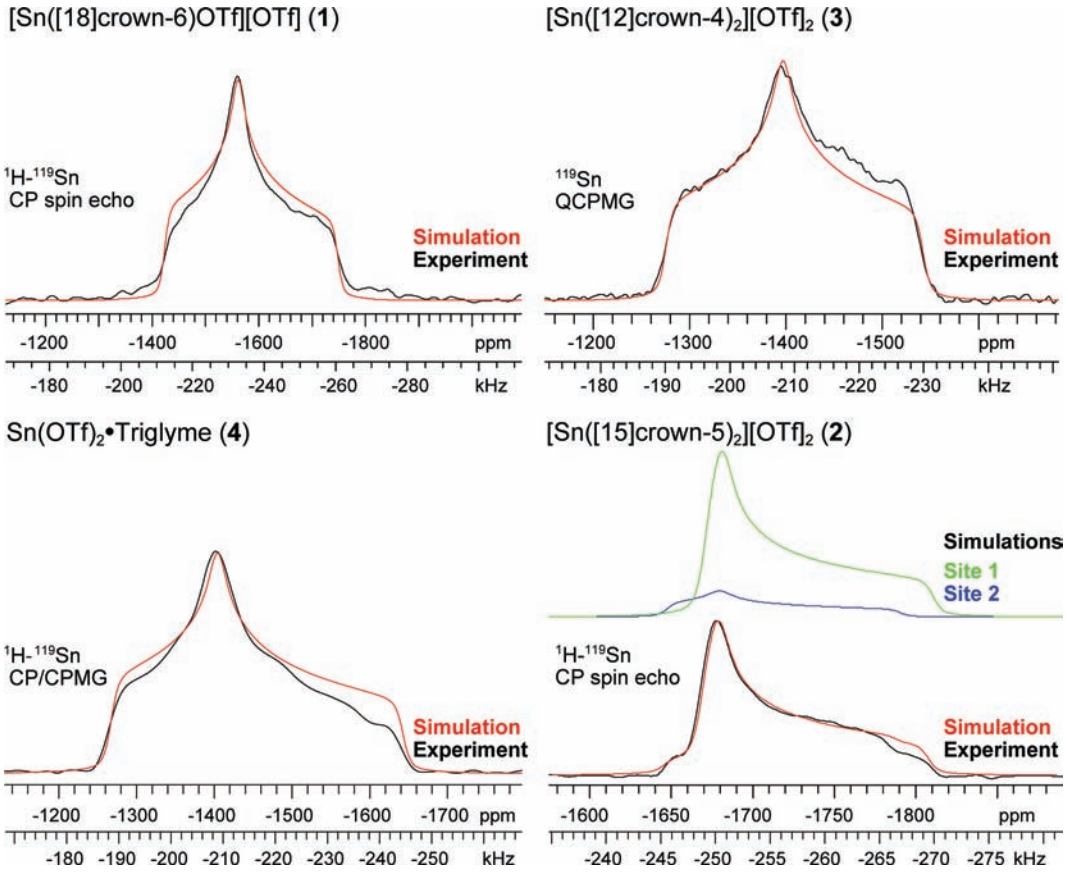

Figure 4. Static ^{119}Sn SSNMR spectra for the triflate complexes **1**−**4** reported in this work. The experimental spectra are depicted with black traces, and the analytical simulations are drawn in red. The spectra of **2** indicate the presence of a second distinct Sn site, which is attributed to a secondary phase of **2**, which contains an excess of free ligand in the crystal lattice;[29] analytical simulations for each of the two overlapping sites are illustrated. MAS ^{119}Sn SSNMR spectra of all complexes are shown in Figure S1.

dx.doi.org/10.1021/ja211135s | J. Am. Chem. Soc. 2012, 134, 4332−4345

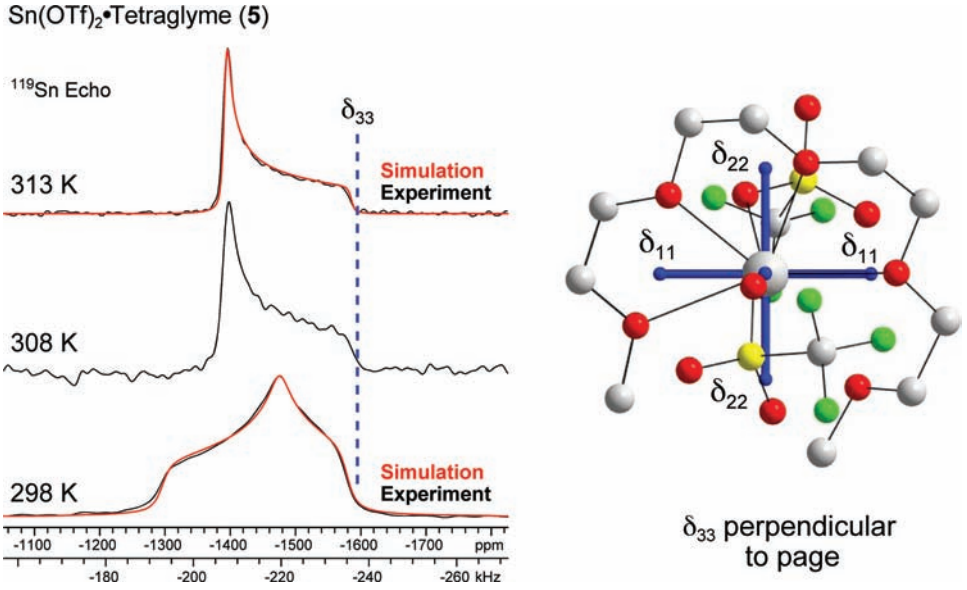

Figure 5. (Left) Static ^{119}Sn SSNMR spectra for the triflate complexes **5** obtained at three different temperatures between 298 and 313 K. The experimental spectra are depicted with black traces, and the analytical simulations are drawn in red. All spectra were obtained with a spin echo pulse sequence. (Right) The CS tensor orientation obtained from DFT calculation on the low temperature structure of **5**.

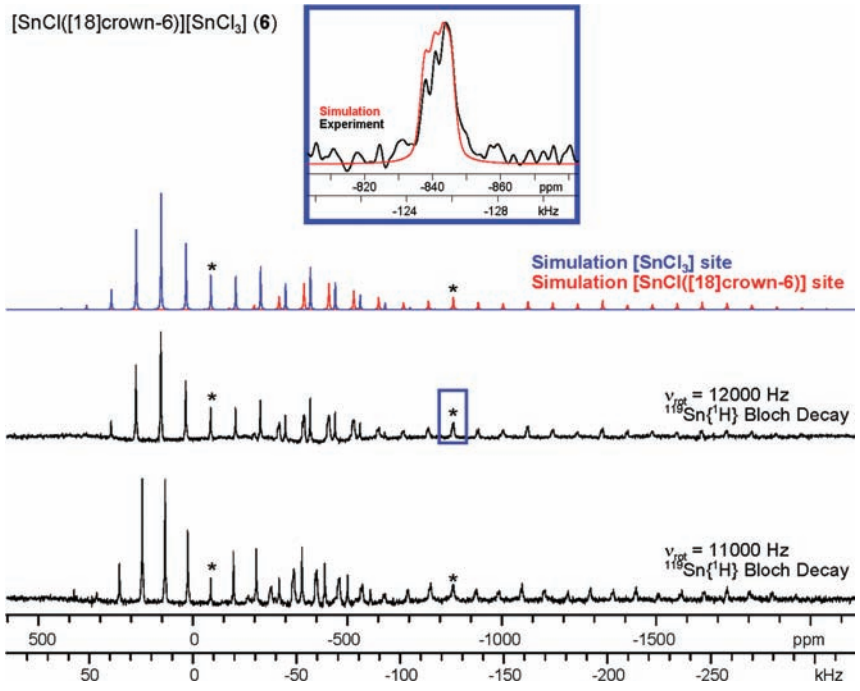

Figure 6. ^{119}Sn MAS SSNMR spectra of **6**. The simulation of the ν_{rot} = 12 000 Hz spectrum includes both the [SnCl([18]crown-6)] site (red trace) and the [$SnCl_3$] site (blue trace). Asterisks denote isotropic peaks. Inset: An expansion of the isotropic peak shows the fine structure of the [SnCl([18]crown-6)] resonances. The simulation illustrates that residual dipolar coupling and indirect spin−spin coupling to $^{35/37}$Cl are most likely responsible for the fine structure. Simulation parameters: $J_{iso}(^{119}Sn-^{35}Cl)$ = 380 Hz, $D(^{119}Sn-^{35}Cl)$ = −307 Hz, ΔJ = 20 Hz, $C_Q(^{35}Cl)$ = −45 MHz, $\eta_Q(^{35}Cl)$ = 0.30, α = 20°, β = 50°. $D(^{119}Sn-^{35}Cl)$ was calculated on the basis of the Sn−Cl bond length observed in the single-crystal X-ray structure of **6**, and the ^{35}Cl EFG tensor parameters were based upon those obtained from DFT calculations. Note that there are large uncertainties (on the order of 20−50%) associated with the values of $J_{iso}(^{119}Sn-^{35}Cl)$, ΔJ, $C_Q(^{35}Cl)$, η_Q, α, and β and employed in the simulations.

Ω is usually observed to increase as well. Among the triflate complexes, **3**−**5** have the most positive values of δ_{iso}, larger values of Ω, and possess the least spherically symmetric Sn coordination environments. These observations imply that the HOMOs ("lone pair") in these complexes are of higher 5p character than in complexes **1** and **2**.

Because of the unexpected appearance of the MAS spectrum of the tetraglyme complex (**5**) at room temperature, VT ^{119}Sn NMR experiments were undertaken (Figure 5). The high temperature spectra (308 and 315 K) exhibit a slightly reduced Ω, and a skew (κ) of approximately +1, which indicates that the CS tensor is axially symmetric (i.e., $\delta_{11} = \delta_{22}$). The spectrum

dx.doi.org/10.1021/ja211135s | J. Am. Chem. Soc. 2012, 134, 4332−4345

Table 3. Experimental and Calculated ^{119}Sn Chemical Shielding Tensor Parameters[a]

compound	method	geom.[b]	σ_{iso} (ppm)	δ_{iso} (ppm)	Ω (ppm)	κ	δ_{11} (ppm)	δ_{22} (ppm)	δ_{33} (ppm)
[Sn([18]crown-6)OTf][OTf] (**1**)	expt.			−1578(2)	325(20)	0.15(5)	−1424	−1562	−1749
	DFT/QZ4P[c]	X	4353	−1799	589	0.30	−1534	−1741	−1799
[Sn([15]crown-5)$_2$][OTf]$_2$ (**2**)	expt. (site 1)			−1721(2)	140(10)	0.85(10)	−1671	−1681	−1811
[Sn([15]crown-5)$_2$][OTf]$_2$ (**2**)	expt. (site 2)			−1706(2)	143(10)	0.55(5)	−1647	−1680	−1791
[Sn([15]crown-5)$_2$]$^{2+}$ [d]	DFT/QZ4P	X	4472	−1918	376	0.65	−1770	−1836	−2147
	DFT/QZ4P	O	4454	−1899	339	0.55	−1761	−1837	−2100
[Sn([12]crown-4)$_2$][OTf]$_2$ (**3**)	expt.			−1405(2)	267(10)	0.09(5)	−1275	−1398	−1539
[Sn([12]crown-4)$_2$]$^{2+}$	DFT/QZ4P	X	4163	−1609	240	−0.09	−1486	−1616	−1725
	DFT/QZ4P	O	4164	−1609	224	−0.38	−1483	−1638	−1707
Sn(OTf)$_2$·triglyme (**4**)	expt.			−1436(1)	375(20)	0.27(4)	−1258	−1400	−1649
	DFT/QZ4P	X	4079	−1524	644	0.29	−1233	−1462	−1877
Sn(OTf)$_2$·tetraglyme (**5**)	expt. (high *T*)			−1457(1)	195(15)	0.96(4)	−1391	−1395	−1586
	expt. (low *T*)			−1448(1)	283(15)	−0.26(5)	−1294	−1472	−1577
	DFT/QZ4P	X	4249	−1694	427	0.17	−1493	−1671	−1920
[**Sn**Cl([18]crown-6)][SnCl$_3$] (**6**)	expt.			−840(5)	1700(150)	1.00(15)	−239	−341	−1939
	DFT/QZ4P	X	3562	−1008	2269	0.99	−246	−262	−2515
[SnCl([18]crown-6)][**Sn**Cl$_3$] (**6**)	expt.			−58(2)	814(100)	1.00(15)	228	190	−588
	DFT/QZ4P	X	2607	−53	821	0.83	244	173	−577
SnCl$_2$[e]	expt.			−916(1)	347(10)	0.59(4)	−777	−848	−1124
Sn(OTf)$_2$	expt.			−1418(2)	517(10)	0.96(5)	−1242	−1253	−1759
SnO[92]	expt.			−208(7)	975(15)	1.00	117	117	−858
SnMe$_4$	expt.			0					
	DFT/QZ4P	O	2554	0	0				

[a]The CS tensor is defined by three principal components ordered such that $\delta_{11} \geq \delta_{22} \geq \delta_{33}$. $\delta_{iso} = (\delta_{11} + \delta_{22} + \delta_{33})/3$. $\Omega = \delta_{11} - \delta_{33}$. $\kappa = 3(\delta_{22} - \delta_{iso})/\Omega$. The uncertainties associated with the last digit of the experimental parameters are shown in brackets. [b]"X" refers to calculations using the X-ray structure derived from the single-point geometry, and "O" refers to calculations employing geometry-optimized structures. [c]An all-electron quadruple-ζ doubly polarized (QZ4P) basis set was employed for Sn as indicated. An all-electron triple-ζ doubly polarized (TZ2P) basis set was employed on all other atoms in all cases. Results using the TZ2P basis set on Sn are found in the Supporting Information. [d]In cases where a tin-containing ion is specified, the triflate groups were omitted from calculations. [e]Refer to the Supporting Information for details.

obtained at low temperature (298 K) has a larger Ω and nonaxial κ (−0.26), which is consistent with the theoretical CS tensor obtained from DFT calculations on a model derived from the low temperature single-crystal X-ray structure. In both the high and the low temperature spectra, the position of δ_{33} is the same, while δ_{22} and δ_{11} become equivalent at high temperature, which suggests that there may be a dynamic molecular motion that averages δ_{11} and δ_{22}. The theoretical CS tensor orientationhas δ_{11} and δ_{22} oriented in the O_5 plane of the tetraglyme ligand (Figure 5); hence there is a dynamic reorientation of either the tetraglyme ligand, or the whole molecule, around the pseudoaxis formed by the triflates.[103]

3.4. Cyclic Voltammetry. Cyclic voltammetry (CV) is used to assess the impact of ligands on the relative redox properties of transition metal complexes, in which the relevant electrons are located in d-orbitals and may not affect the overall structure. For the p-block metals, the population of p-orbitals (especially starting from a putative s^2p^0 valence electron configuration) usually has an obvious effect on the structure of the compound, and CV is often not needed to assess the oxidation state or valence state of the metal. Regardless, we sought to determine the effect of the different polyether ligands on the oxidation potential of the tin atom with which they interact and to assess, in particular, if there is any obvious correlation between the oxidation potential of the tin atom and any of the spectral and/or structural data described above. Thus, the CVs of CH_2Cl_2 solutions of complexes **1**−**5** were obtained to assess the relative stabilities of divalent tin atoms. Because we are most interested in the oxidation of the Sn^{2+} to Sn^{4+}, all of the voltammograms were recorded using glassy carbon electrodes to observe the anodic peak for the couple, which is often not observed when platinum electrodes are employed.[104,105]

Every signal observed in the CVs of complexes **1**−**5** (Figure 7) is irreversible under all conditions investigated; therefore, the potentials reported in Table 4 are those obtained by sweeping initially toward either more positive potentials (for Sn^{2+} oxidation) or negative potentials (for Sn^{2+} reduction). Perhaps the most interesting observation is that compounds **2** and **3** do not feature any observable signal corresponding to the oxidation from Sn^{2+} to Sn^{4+}. Given that the oxidation of tin(II) chloride was determined to occur through an inner sphere mechanism that requires the tin atom to be bridged to the anode,[104] it is perhaps not surprising that the completely surrounded tin atoms in both complexes do not give rise to detectable oxidation currents under these conditions. Furthermore, compound **1** exhibits a significant oxidation current at roughly +1600 mV, which is considerably higher than the corresponding value for unligated Sn(OTf)$_2$. In contrast, both of the glyme complexes **4** and **5** are considerably easier to oxidize than any of the crown ether complexes. These observations are somewhat counterintuitive, given that complex **2**, which features a tin atom surrounded by ligands containing 10 oxygen donor sites, might be expected to be the most electron-rich complex investigated and the most easily oxidized. Furthermore, despite having 6 donor atoms in the ligand, the [18]crown-6 complex **1** is the least easily oxidized of any of the single-ligand complexes, whereas oxidation of the two podand complexes require potentials similar to, or lower than, that of "free" Sn(OTf)$_2$.

Overall, the CV data suggest that the observed (and unobserved) Sn^{2+} to Sn^{4+} oxidation potentials are attributable to the steric properties of the ligands about the tin atom rather

dx.doi.org/10.1021/ja211135s | J. Am. Chem. Soc. 2012, 134, 4332−4345

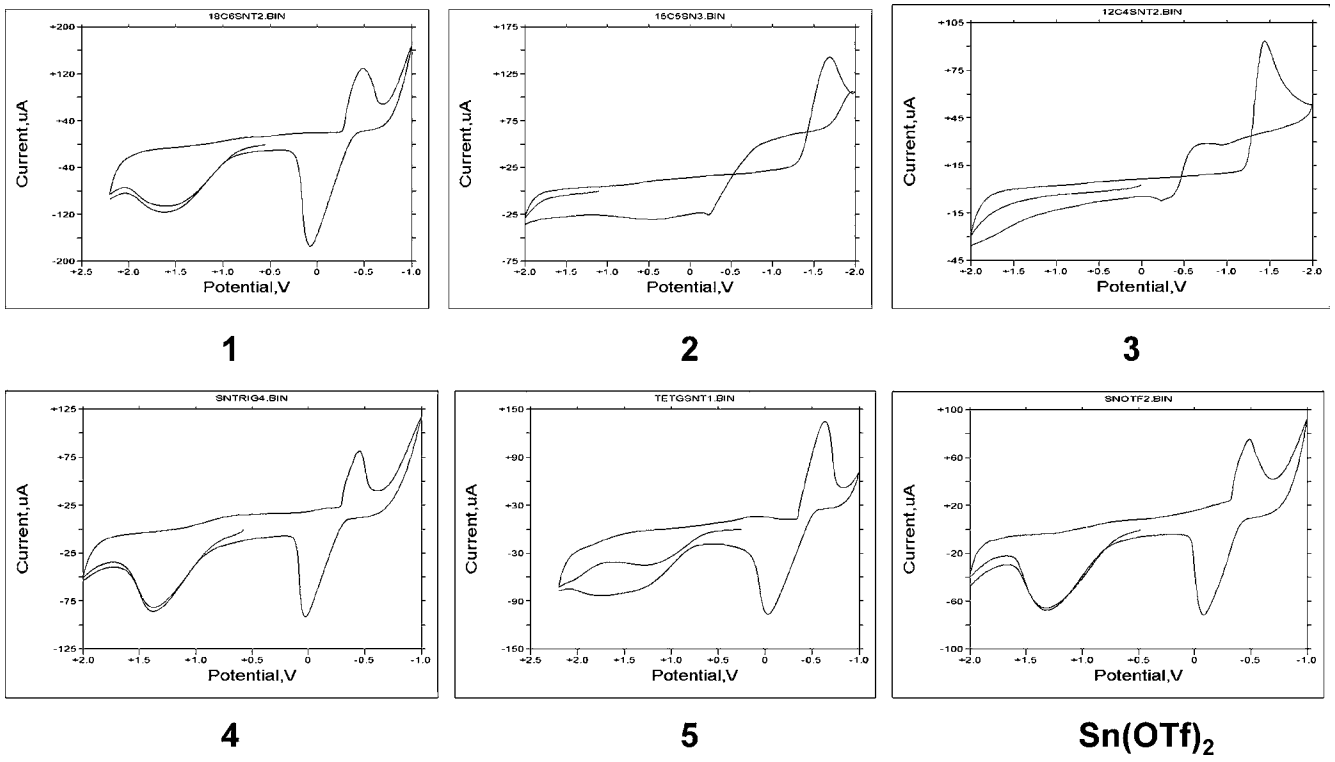

Figure 7. Representative cyclic voltammograms for solutions of triflate complexes **1**–**5** reported in this work and $Sn(OTf)_2$.

Table 4. Summary of Cyclic Voltammetry Data Obtained for the Ligand Complexes of $Sn(OTf)_2$

	initial sweep positive		initial sweep negative	
complex	$E_{A(2+\rightarrow4+)}$ (mV)[a,b]	$E_{C(4+\rightarrow2+)}$ (mV)[b]	$E_{A(0\rightarrow2+)}$ (mV)	$E_{C(2+\rightarrow0)}$ (mV)
1	1600	n/o	90	−480
2	n/o	n/o	−220	−1690
3	n/o	n/o	30	−1270
4	1380	n/o	30	−450
5	1240	n/o	−30	−630
$Sn(OTf)_2$	1320	n/o	−80	−500

[a]Potentials were referenced using a $Ag/AgNO_3$ electrode. [b]E_A indicates the anodic potential, and E_C indicates the cathodic potential for the redox couple indicated in parentheses. "n/o" indicates not observed.

than providing direct evidence about the relative energy of the valence electrons on tin. The most encapsulating coordination environments, such as in **2** and **3**, preclude observation of an oxidation current. For the single-ligand complexes, in which the tin atom is not completely surrounded, the data are most consistent with there being a correlation between the percentages of s-character on the tin[106] atoms and the oxidation potentials of the complexes. Specifically, complexes in which the valence electrons on tin have a greater s-character require more energy to become oxidized. Therefore, it appears as if it is the nature of the interaction between the metal and the ligand and the manner in which the ligand perturbs the valence electrons on the metal, rather than simply the donor ability of the ligand, that determines the oxidation potential of the complex.[107] The nature of these interactions and effects are investigated computationally in the following section.

3.5. Computational Investigations. As compiled in Table 5, we examined several different aspects of the electronic structures of models of complexes **1**–**6** using MP2 and TD-DFT calculations to determine if there is any correlation to the experimentally observed properties. Most of the electronic properties were evaluated at the MP2 level of theory on model compounds in which the relative positions of the heavy atoms were fixed in the geometry observed by single-crystal X-ray diffraction, and in which the hydrogen atoms were placed in idealized positions using Gaussview.

Several important observations can be made on the basis of the computed data in Table 5 for the model tin(II) polyether complexes. The NBO charge on the Sn atom is almost always the same (+1.64 ± 0.03 au) for every complex of $Sn(OTf)_2$ regardless of the identity of the polyether ligand or the overall charge of the model in which it is located. These values suggest that there is a relatively small (ca. −0.36 au) total transfer of charge from all of the ligands in the coordination spheres to the metals. The sums of the Wiberg bond indices (WBI) on the tin atoms are likewise remarkably similar and small (0.75 ± 0.06) for all of the triflate complexes. Taken together, these results are consistent with the conclusion from the Mössbauer investigations that the tin atom in each of the triflate complexes behaves like a free Sn^{2+} dication. In sharp contrast to the triflate complexes, the charge on tin is significantly less (+1.47 au) in **6′**, the model containing the chlorine substituent, and the sum of the WBIs for the tin atom in that complex (1.018) is markedly larger. More importantly, it is found that while no Sn−OTf bonds are identified by the NBO analysis for any of triflate model complexes, a Sn−Cl bond is identified for model complex **6′**. The bond is quite polar, featuring ca. 89% contribution from orbitals on the chlorine atom, but its observation clearly illustrates that there is a fundamental difference between the superficially analogous complexes **1′** and **6′**.

dx.doi.org/10.1021/ja211135s | J. Am. Chem. Soc. 2012, 134, 4332–4345

Table 5. Summary of Electronic Structure Analyses for the Single-Point MP2 and TD-DFT Calculations on Models of the Compounds Reported in This Work (X = OTf, Cl)

model complex	Q(Sn)[a]	LP(Sn) %5s[b]	$E_{LP(Sn)}$ (eV)[c]	ΔE_{H-L} (eV)[d]	WBI[e] (M−O_{ligand}) range	WBI[e] (M−X)	WBI[e] (M) total	trans[f] (eV)
Sn^{2+} Models[g]								
$[Sn(12cr4)_2]^{2+}$ (**3′**)	1.64	97.1	−18.54	12.65	0.062−0.097		0.774	4.2666
$[Sn(15cr5)_2]^{2+}$ (**2′**)	1.61	99.7	−18.35	12.47	0.052−0.080		0.810	4.1432
SnX^+ Models								
$[(18cr6)Sn-OTf]^+$ (**1′**)	1.66	95.6	−16.58	12.41	0.047−0.090	0.170	0.687	4.1157
$[(18cr6)Sn-Cl]^+$ (**6′**)	1.47	93.9	−15.59	12.47	0.057−0.080	0.536	1.018	4.4283
SnX_2 Models								
(18cr6)·$Sn(OTf)_2$ (**1″**)	1.63	97.8	−12.49	13.04	0.042−0.088	0.090;0.133	0.781	4.4016
(trig)·$Sn(OTf)_2$ (**4′**)	1.67	95.9	−13.26	12.16	0.058−0.1015	0.090;0.137	0.701	3.8524
(tetrag)·$Sn(OTf)_2$ (**5′**)	1.63	97.4	−12.55	12.72	0.041−0.095	0.110;0.121	0.783	4.2286

[a]NBO charge on the metal atom. [b]NBO percentage of 5s character in the "lone pair" orbital on the metal atom. [c]NBO energy of the "lone pair" on Sn. [d]SCF HOMO−LUMO energy difference. [e]NBO Wiberg bond index for the bonds indicated. [f]TD-DFT lowest energy transition. [g]The data are subdivided on the basis of the overall charge of the models employed.

Similarly, it is apparent that the calculated percentage of 5s character in the "lone pair" of electrons on Sn is very high (>90%) for each of the divalent tin model complexes; however, there are some notable differences. As one may anticipate, the percentage of 5s character for the "lone pair" is highest (99.7%) for the [15]crown-5 sandwich model complex **2′**, which most closely approximates spherical symmetry. The "lone pair" in the [12]crown-4 sandwich model complex **3′** is found to be around 97.1% 5s, and all of the other model triflate complexes have 5s percentages that exceed 95%. While the magnitude of the difference is not tremendous, it is again the chloride model complex **6′** that is the outlier: this complex features the smallest percentage (93.9%) of s-character for the two nonbonding valence electrons. Although s−p mixing is not a prerequisite for stereochemical activity of a "lone pair",[108,109] lower percentages of s character appear to correlate with higher reactivity for the systems herein.

The energies of the "lone pairs" of electrons on the tin atom in each model complex, as identified by the NBO analysis, were also examined to determine if there is any correlation between their energies and the tin coordination environments. The energies of these orbitals are found to be very similar to each other for triflate models of the same overall charge: for example, the energies for the two dicationic models **2′** and **3′** are virtually identical. The only major difference observed is, again, between the triflate complex **1′** and the chloride complex **6′**. The lone pair in **6′** is more than 1 eV less stable than that of **1′**, which suggests that the chloride species should be more reactive as an electron donor; this result concurs with our observations of the related univalent indium systems.[25] Furthermore, these data indicate that the complex with the highest charge on the tin atom is not necessarily the most reactive.

It must also be emphasized that the frontier orbitals in all of the models are almost exclusively based on tin. The molecular orbital that corresponds to the "lone pair" of valence electrons on the tin atom is the highest occupied molecular orbital (HOMO) for each of the model complexes examined. Furthermore, all of the lowest unoccupied molecular orbitals (LUMOs) on each of the complexes are primarily composed of the formally vacant 5p orbitals on tin; the relevant orbitals for model complexes **1′** and **6′** are illustrated in Figure 8.[110] Despite the different absolute energies found for the HOMOs described above, which suggest that the chlorinated compound is more basic, there does not appear to be any marked difference in the HOMO−LUMO gaps for any of the complexes (as calculated using the MP2 method)

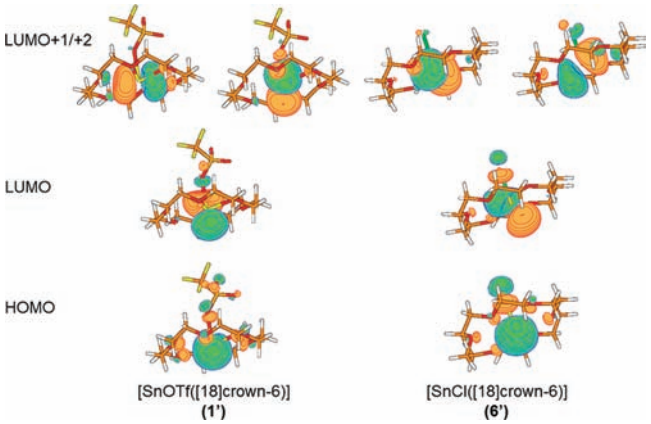

Figure 8. Depictions of selected MP2 frontier orbitals for model complexes **1′** and **6′**.

nor in the lowest energy electronic transitions (as calculated with TD-DFT using the B3PW91 method).

One very important observation gleaned from the examination of the molecular orbitals in model complexes **1′** and **6′** is the presence of an obvious Cl−Sn bonding orbital in the latter (Figure 9). In contrast, no corresponding TfO−Sn bonding orbital is found in **1′**; therefore, both the MP2 molecular orbitals and the NBO analysis point to the conclusion that there really is a substantial difference between the bonding in the two superficially analogous ions. This observation provides a rationale for the considerable differences in the features observed in both the Mössbauer spectra and the ^{119}Sn SSNMR spectra. Moreover, the presence of the more covalent bond between the substituent and the tin atom also explains the decreased stability of the "lone pair" of electrons on tin (Scheme 3).

Given the apparently different nature of the X−Sn bonding (X = OTf, Cl) between model complexes **1′** and **6′**, we examined the Laplacian, $\nabla^2\rho$, of the MP2 electron density for each of the complexes (Figure 10). It is clear that the electron density in **1′** is consistent with the description of the complex as being a contact ion pair, whereas the region between the tin atom and the chlorine atom in **6′** has a region of electron density concentration between the two atoms that is consistent with the presence of a bond between tin and chlorine. Therefore, the conclusions obtained through analysis of the topology of the electron density are in accord with those derived from the various analyses of the molecular orbitals and the spectroscopic

dx.doi.org/10.1021/ja211135s | J. Am. Chem. Soc. 2012, 134, 4332−4345

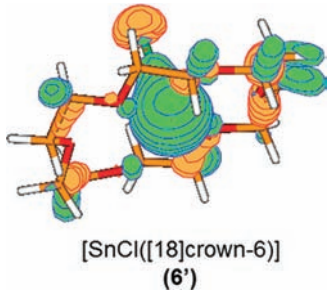

Figure 9. Depiction of the Sn−Cl "bonding" MP2 orbital for model complex **6′**.

Scheme 3. Simplified MO Diagram ($C_{\infty v}$ Symmetry) Illustrating Why Covalent Bonding Destabilizes the "Lone Pair" MO on a Divalent Tin Dication

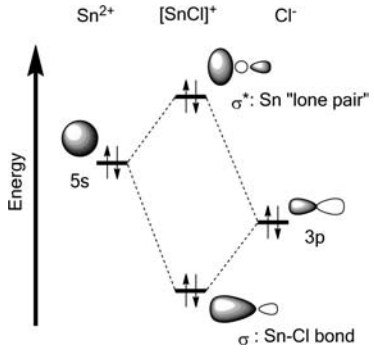

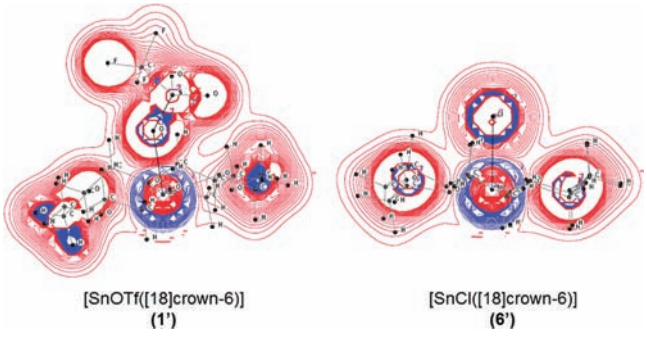

Figure 10. Contour diagrams depicting the Laplacian, $\nabla^2\rho$, of the MP2 electron density for model complexes **1′** and **6′**. Contours depicted in red indicate regions of negative charge depletion (decreased electron density), and those in blue indicate regions of negative charge concentration (increased electron density).

data: the nature of the interaction between the tin atom and the triflate substituent truly is different from the interaction with the chloride substituent.

Finally, in light of all of the preceding data, it is worth clarifying why the more covalent bond with chlorine destabilizes the "lone pair" on the tin atom. As illustrated in Scheme 3, the "lone pair" MO in $[SnCl]^+$ is formally the result of the antibonding interaction between the filled $5s^2$ orbital on a free Sn^{2+} ion and a filled 3p orbital on a free Cl^- anion. In this context, it is apparent that a stronger, more covalent interaction must result in a higher energy, more reactive "lone pair" on tin than is present in the free ion.

4. CONCLUSIONS

The structural, spectroscopic, and computational results presented in this work clearly demonstrate that there are dramatic differences between the behavior of the nonbonding electrons in low-valent complexes. These differences can be rationalized on the basis of the nature of the multidentate ligand present and, more importantly, on the properties of the substituent that are bound to the low-valent metal. In particular, triflate substituents produce highly ionic contact ion pairs (featuring Sn^{2+} dications), whereas chloride substituents generate species with covalently bonded $[Sn-Cl]^+$ cations: our investigations provide an explanation for the differing electrochemical behavior of solutions of $SnCl_2$ and $Sn(OTf)_2$ in ionic liquids reported by Compton and co-workers, who proposed similar speciation.[111] More generally, this observation provides insight as to how coordinating counterions can destabilize electron-rich species and thus why very weakly coordinating counterions are sometimes required to isolate particularly reactive low-valent species such as Ga(I).[112]

Despite the differences, all of the investigations also illustrate that the nonbonding electrons on the tin atom in each complex reside in orbitals that are almost exclusively of 5s character and the various polyether ligands appear to perturb those electrons only mildly. The properties of the sandwich-like complexes **2** and **3** are consistent with the least perturbation from an ideal $5s^2$ electron configuration, whereas the properties of the [18]crown-6 complexes **1**, and to an even greater extent **6**, appear to be the most perturbed. The increased perturbation caused by the [18]crown-6 ligand in comparison to either the free salt or the sandwich complexes provides a rationale for the observed differences in oxidative addition reactions of the related In^I complexes.

Acyclic podand ligands also appear to be suitable for the stabilization and/or solubilization of low-valent p-block reagents, and the properties of the resultant complexes are intermediate between those of the free salt and the [18]crown-6 complexes. We surmise that the more flexible nature of such ligands in comparison to their more constrained cyclic relatives may explain this observation.

Overall, this work provides a rationale for why ligands with multiple weak donors are useful for the stabilization, isolation, or solubilization of electron-rich main group species. Consequently, these results also provide an explanation as to why stronger donors, such as tetramethylethylenediamine (TMEDA), which are often employed in an attempt to solubilize low-valent reagents, result in the decomposition of the species.[113,114] Finally, the dramatically different bonding and properties of the chloride complexes with respect to their triflate analogues suggest that the relatively more stable triflate complexes may be conveniently rendered more reactive simply through the addition of better donors. Investigations to probe and exploit such behavior are currently underway.

■ ASSOCIATED CONTENT

Supporting Information

Crystallographic information files, summary of computational results and complete references for the Gaussian packages, solid-state ^{13}C NMR spectra, and additional information regarding the solid-state NMR experiments. This material is available free of charge via the Internet at http://pubs.acs.org.

■ AUTHOR INFORMATION

Corresponding Author

cmacd@uwindsor.ca

Notes

The authors declare no competing financial interest.

■ ACKNOWLEDGMENTS

We thank the Natural Science and Engineering Research Council (NSERC) of Canada for funding (C.L.B.M., S.H.E., R.W.S.) and scholarships (A.J.R., W.W.F.). We thank the Government of Ontario for scholarships (B.F.T.C.) and Early Researcher Awards (C.L.B.M., R.W.S.). We thank the Canada Foundation for Innovation, the Ontario Innovation Trust, and the Ontario Research and Development Challenge Fund for support of the University of Windsor's Centre for Catalysis and Materials Research and the Solid-State NMR Centre. We are indebted to Prof. I. Nowik for significant help in ME data reduction and numerous fruitful discussions of the data.

■ REFERENCES

(1) Parkin, G. *J. Chem. Educ.* **2006**, *83*, 791.
(2) Jansen, M.; Wedig, U. *Angew. Chem. Int. Ed.* **2008**, *47*, 10026.
(3) Macdonald, C. L. B.; Ellis, B. D. In *Encyclopedia of Inorganic Chemistry*, 2nd ed.; King, R. B., Ed.; John Wiley & Sons Ltd.: New York, 2005.
(4) Arnold, J. *Dalton Trans.* **2008**, 4334.
(5) Chivers, T.; Konu, J. *Comments Inorg. Chem.* **2009**, *30*, 131.
(6) Fischer, R. A.; Weiss, J. *Angew. Chem. Int. Ed.* **1999**, *38*, 2831.
(7) Dao, H. T.; Schneider, U.; Kobayashi, S. *Chem. Commun.* **2011**, *47*, 692.
(8) Aksu, Y.; Driess, M. *Angew. Chem. Int. Ed.* **2009**, *48*, 7778.
(9) Welsch, S.; Bodensteiner, M.; Dusek, M.; Sierka, M.; Scheer, M. *Chem.—Eur. J.* **2010**, *16*, 13041.
(10) Schnepf, A.; Schnockel, H. *Angew. Chem. Int. Ed.* **2002**, *41*, 3533.
(11) Schnockel, H. *Chem. Rev.* **2010**, *110*, 4125.
(12) Clyburne, J. A. C.; McMullen, N. *Coord. Chem. Rev.* **2000**, *210*, 73.
(13) Bourget-Merle, L.; Lappert, M. F.; Severn, J. R. *Chem. Rev.* **2002**, *102*, 3031.
(14) Nagendran, S.; Roesky, H. W. *Organometallics* **2008**, *27*, 457.
(15) Asay, M.; Jones, C.; Driess, M. *Chem. Rev.* **2011**, *111*, 354.
(16) Jones, C. *Coord. Chem. Rev.* **2010**, *254*, 1273.
(17) Kuhl, O. *Coord. Chem. Rev.* **2004**, *248*, 411.
(18) Wolff, M.; Harmening, T.; Pottgen, R.; Feldmann, C. *Inorg. Chem.* **2009**, *48*, 3153.
(19) Kuate, A. C. T.; Schurmann, M.; Schollmeyer, D.; Hiller, W.; Jurkschat, K. *Chem.—Eur. J.* **2010**, *16*, 8140.
(20) Macdonald, C. L. B.; Corrente, A. M.; Andrews, C. G.; Taylor, A.; Ellis, B. D. *Chem. Commun.* **2004**, 250.
(21) Andrews, C. G.; Macdonald, C. L. B. *Angew. Chem., Int. Ed.* **2005**, *44*, 7453.
(22) Cooper, B. F. T.; Andrews, C. G.; Macdonald, C. L. B. *J. Organomet. Chem.* **2007**, *692*, 2843.
(23) Cooper, B. F. T.; Macdonald, C. L. B. *J. Organomet. Chem.* **2008**, *693*, 1707.
(24) Cooper, B. F. T.; Macdonald, C. L. B. *New J. Chem.* **2010**, *34*, 1551.
(25) Cooper, B. F. T.; Hamaed, H.; Friedl, W. W.; Stinchcombe, M. R.; Schurko, R. W.; Macdonald, C. L. B. *Chem.—Eur. J.* **2011**, *17*, 6148.
(26) Rupar, P. A.; Bandyopadhyay, R.; Cooper, B. F. T.; Stinchcombe, M. R.; Ragogna, P. J.; Macdonald, C. L. B.; Baines, K. M. *Angew. Chem. Int. Ed.* **2009**, *48*, 5155.
(27) Cheng, F.; Hector, A. L.; Levason, W.; Reid, G.; Webster, M.; Zhang, W. J. *Angew. Chem. Int. Ed.* **2009**, *48*, 5152.
(28) Rupar, P. A.; Staroverov, V. N.; Baines, K. M. *Science* **2008**, *322*, 1360.
(29) Bandyopadhyay, R.; Cooper, B. F. T.; Rossini, A. J.; Schurko, R. W.; Macdonald, C. L. B. *J. Organomet. Chem.* **2010**, *695*, 1012.
(30) Herber, R. H.; Smelkinson, A. E. *Inorg. Chem.* **1978**, *17*, 1023.
(31) Drew, M. G. B.; Nicholson, D. G. *J. Chem. Soc., Dalton Trans.* **1986**, 1543.
(32) Pangborn, A. B.; Giardello, M. A.; Grubbs, R. H.; Rosen, R. K.; Timmers, F. J. *Organometallics* **1996**, *15*, 1518.
(33) *SMART*; Bruker AXS Inc.: Madison, WI, 2001.
(34) *SAINTPlus*; Bruker AXS Inc.: Madison, WI, 2001.
(35) *SADABS*; Bruker AXS Inc.: Madison, WI, 2001.
(36) Altomare, A.; Burla, M. C.; Camalli, M.; Cascarano, G. L.; Giacovazzo, C.; Guagliardi, A.; Moliterni, A. G. G.; Polidori, G.; Spagna, R. *J. Appl. Crystallogr.* **1999**, *32*, 115.
(37) Sheldrick, G. M. *Acta Crystallogr., Sect. A* **2008**, *64*, 112.
(38) Farrugia, L. J. *J. Appl. Crystallogr.* **1999**, *32*, 837.
(39) Sheldrick, G. M. *SHELXTL*; Bruker AXS Inc.: Madison, WI, 2001.
(40) Spek, A. L. *J. Appl. Crystallogr.* **2003**, *36*, 7.
(41) Mansell, S. M.; Herber, R. H.; Nowik, I.; Ross, D. H.; Russell, C. A.; Wass, D. F. *Inorg. Chem.* **2011**, *50*, 2252.
(42) Cohen, S.; Ma, J. X.; Butenschon, H.; Herber, R. H. *Dalton Trans.* **2009**, 6606.
(43) http://www.megadaq.com.
(44) A spectrum of **1** taken after storing an O-ring closed sample at ambient temperature and in air suggests that most, if not all, of the Sn(IV) impurity arises from adventitious hydrolysis.
(45) Harris, R. K.; Becker, E. D.; De Menezes, S. M. C.; Goodfellow, R.; Granger, P. *Pure Appl. Chem.* **2001**, *73*, 1795.
(46) Earl, W. L.; Vanderhart, D. L. *J. Magn. Reson.* **1982**, *48*, 35.
(47) Peersen, O. B.; Wu, X. L.; Kustanovich, I.; Smith, S. O. *J. Magn. Reson., Ser. A* **1993**, *104*, 334.
(48) Peersen, O. B.; Wu, X. L.; Smith, S. O. *J. Magn. Reson., Ser. A* **1994**, *106*, 127.
(49) Larsen, F. H.; Jakobsen, H. J.; Ellis, P. D.; Nielsen, N. C. *J. Phys. Chem. A* **1997**, *101*, 8597.
(50) Hung, I.; Rossini, A. J.; Schurko, R. W. *J. Phys. Chem. A* **2004**, *108*, 7112.
(51) Siegel, R.; Nakashima, T. T.; Wasylishen, R. E. *J. Phys. Chem. B* **2004**, *108*, 2218.
(52) Larsen, F. H.; Skibsted, J.; Jakobsen, H. J.; Nielsen, N. C. *J. Am. Chem. Soc.* **2000**, *122*, 7080.
(53) Lefort, R.; Wiench, J. W.; Pruski, M.; Amoureux, J. P. *J. Chem. Phys.* **2002**, *116*, 2493.
(54) Bennett, A. E.; Rienstra, C. M.; Auger, M.; Lakshmi, K. V.; Griffin, R. G. *J. Chem. Phys.* **1995**, *103*, 6951.
(55) Eichele, K. *WSolids: Solid-State NMR Spectrum Simulation*, V1.20.15; Universitat Tubingen: Tubingen, Germany, 2011.
(56) Herzfeld, J.; Berger, A. E. *J. Chem. Phys.* **1980**, *73*, 6021.
(57) Frisch, M. J.; et al. *Gaussian 03*, revision D.01; Gaussian, Inc.: Pittsburgh, PA, 2003.
(58) Frisch, M. J.; et al. *Gaussian 09*, revision A1; Gaussian, Inc.: Pittsburgh, PA, 2009.
(59) Becke, A. D. *J. Chem. Phys.* **1993**, *98*, 5648.
(60) Perdew, J. P.; Wang, Y. *Phys. Rev. B* **1992**, *45*, 13244.
(61) Bergner, A.; Dolg, M.; Kuchle, W.; Stoll, H.; Preuss, H. *Mol. Phys.* **1993**, *80*, 1431.
(62) Reed, A. E.; Curtiss, L. A.; Weinhold, F. *Chem. Rev.* **1988**, *88*, 899.
(63) Godbout, N.; Salahub, D. R.; Andzelm, J.; Wimmer, E. *Can. J. Chem.* **1992**, *70*, 560.
(64) Sosa, C.; Andzelm, J.; Elkin, B. C.; Wimmer, E.; Dobbs, K. D.; Dixon, D. A. *J. Phys. Chem.* **1992**, *96*, 6630.
(65) Schaftenaar, G.; Noordik, J. H. *J. Comput.-Aided Mol. Des.* **2000**, *14*, 123.
(66) Schreckenbach, G.; Ziegler, T. *J. Phys. Chem.* **1995**, *99*, 606.
(67) Schreckenbach, G.; Ziegler, T. *Int. J. Quantum Chem.* **1997**, *61*, 899.
(68) Wolff, M.; Harmening, T.; Pottgen, R.; Feldmann, C. *Inorg. Chem.* **2009**, *48*, 3153.
(69) Guerra, C. F.; Snijders, J. G.; te Velde, G.; Baerends, E. J. *Theor. Chem. Acc.* **1998**, *99*, 391.

(70) Velde, G. T.; Bickelhaupt, F. M.; Baerends, E. J.; Guerra, C. F.; Van Gisbergen, S. J. A.; Snijders, J. G.; Ziegler, T. *J. Comput. Chem.* **2001**, *22*, 931.
(71) *ADF2005.01*; SCM, Theoretical Chemistry, Vrije Universiteit.
(72) Becke, A. D. *Phys. Rev. A* **1988**, *38*, 3098.
(73) Perdew, J. P. *Phys. Rev. B* **1986**, *33*, 8822.
(74) Vosko, S. H.; Wilk, L.; Nusair, M. *Can. J. Phys.* **1980**, *58*, 1200.
(75) Autschbach, J.; Ziegler, T. *Calculation of NMR and EPR Parameters*; Wiley-VCH: Weinheim, 2004; p 249.
(76) Autschbach, J. *Calculation of NMR and EPR Parameters*; Wiley-VCH: Weinheim, 2004; p 227.
(77) van Lenthe, E.; Baerends, E. J.; Snijders, J. G. *J. Chem. Phys.* **1993**, *99*, 4597.
(78) van Lenthe, E.; Baerends, E. J.; Snijders, J. G. *J. Chem. Phys.* **1994**, *101*, 9783.
(79) van Lenthe, E.; van Leeuwen, R.; Baerends, E. J.; Snijders, J. G. *Int. J. Quantum Chem.* **1996**, *57*, 281.
(80) Ditchfield, R. *Mol. Phys.* **1974**, *27*, 789.
(81) Allen, F. H. *Acta Crystallogr., Sect. B: Struct. Crystallogr. Cryst. Chem.* **2002**, *58*, 380.
(82) Herber, R. H.; Carrasquillo, G. *Inorg. Chem.* **1981**, *20*, 3693.
(83) Hough, E.; Nicholson, D. G.; Vasudevan, A. K. *J. Chem. Soc., Dalton Trans.* **1989**, 2155.
(84) Batchelor, R. J.; Ruddick, J. N. R.; Sams, J. R.; Aubke, F. *Inorg. Chem.* **1977**, *16*, 1414.
(85) Ward, M. J.; Rupar, P. A.; Murphy, M. W.; Yiu, Y. M.; Baines, K. M.; Sham, T. K. *Chem. Commun.* **2010**, *46*, 7016.
(86) Schurko, R. W.; Hung, I.; Macdonald, C. L. B.; Cowley, A. H. *J. Am. Chem. Soc.* **2002**, *124*, 13204.
(87) Knop, O.; Palmer, E. M.; Robinson, R. W. *Acta Crystallogr., Sect. A* **1975**, *A 31*, 19.
(88) Knop, O. *Acta Crystallogr., Sect. A* **1976**, *32*, 147.
(89) Akitt, J. W.; McDonald, W. S. *J. Magn. Reson.* **1984**, *58*, 401.
(90) Kennedy, J. D.; McFarlane, W. In *Multinuclear NMR*; Mason, J., Ed.; Plenum: New York, 1987.
(91) Wrackmeyer, B. *Annu. Rep. NMR Spectrosc.* **1999**, *38*, 203.
(92) Cossement, C.; Darville, J.; Gilles, J. M.; Nagy, J. B.; Fernandez, C.; Amoureux, J. P. *Magn. Reson. Chem.* **1992**, *30*, 263.
(93) Ramsey, N. F. *Phys. Rev.* **1950**, *78*, 699.
(94) Ramsey, N. F. *Phys. Rev.* **1951**, *83*, 540.
(95) Ramsey, N. F. *Phys. Rev.* **1952**, *86*, 243.
(96) Komoroski, R. A.; Parker, R. G.; Mazany, A. M.; Early, T. A. *J. Magn. Reson.* **1987**, *73*, 389.
(97) Eichler, B. E.; Phillips, B. L.; Power, P. P.; Augustine, M. P. *Inorg. Chem.* **2000**, *39*, 5450.
(98) Spikes, G. H.; Giuliani, J. R.; Augustine, M. P.; Nowik, I.; Herber, R. H.; Power, P. P. *Inorg. Chem.* **2006**, *45*, 9132.
(99) Brauniger, T.; Ghedia, S.; Jansen, M. *Z. Anorg. Allg. Chem.* **2010**, *636*, 2399.
(100) Briand, G. G.; Smith, A. D.; Schatte, G.; Rossini, A. J.; Schurko, R. W. *Inorg. Chem.* **2007**, *46*, 8625.
(101) Katz, M. J.; Michaelis, V. K.; Agular, P. M.; Yson, R.; Lu, H.; Kaluarachchi, H.; Batchelor, R. J.; Schreckenbach, G.; Kroeker, S.; Patterson, H. H.; Leznoff, D. B. *Inorg. Chem.* **2008**, *47*, 6353.
(102) Greer, B. J. G. B. J.; Michaelis, V. K.; Katz, M. J.; Leznoff, D. B.; Schreckenbach, G.; Kroeker, S. *Chem.—Eur. J.* **2011**, *17*, 3609.
(103) The existence of such dynamic behavior might also explain the poor predicted value of QS for compound **4** in Table 2.
(104) Mandler, D.; Bard, A. J. *J. Electronanal. Chem.* **1991**, *307*, 217.
(105) Leong, T. I.; Hsieh, Y. T.; Sun, I. W. *Electrochim. Acta* **2011**, *56*, 3941.
(106) As inferred on the basis of the IS values observed in the Mössbauer experiments and the magnitudes of Ω observed in the Sn-119 SSNMR spectra.
(107) The nature of the polyether ligand present also affects the potentials required for metal deposition and "stripping"; some details are provided in the Supporting Information.
(108) Mudring, A. V.; Rieger, F. *Inorg. Chem.* **2005**, *44*, 6240.
(109) Mudring, A. V. *Eur. J. Inorg. Chem.* **2007**, 882.
(110) Because all of the frontier orbitals are almost exclusively tin-based, the computational examination of the various electronic properties described above should indeed provide information that correlates with the experimental investigations that use the tin atom as a probe.
(111) Martindale, B. C. M.; Jones, S. E. W.; Compton, R. G. *Phys. Chem. Chem. Phys.* **2010**, *12*, 1827.
(112) Slattery, J. M.; Higelin, A.; Bayer, T.; Krossing, I. *Angew. Chem. Int. Ed.* **2010**, *49*, 3228.
(113) Green, S. P.; Jones, C.; Stasch, A. *Angew. Chem. Int. Ed.* **2007**, *46*, 8618.
(114) Green, S. P.; Jones, C.; Stasch, A. *Chem. Commun.* **2008**, 6285.